PHYSICAL REVIEW A **79**, 012305 (2009)

Direct observation of quantum criticality in Ising spin chains

Jingfu Zhang,[1,*] Fernando M. Cucchietti,[2,†] C. M. Chandrashekar,[1] Martin Laforest,[1] Colm A. Ryan,[1] Michael Ditty,[1]
Adam Hubbard,[1] John K. Gamble,[3] and Raymond Laflamme[1,4,‡]
[1]*Institute for Quantum Computing and Department of Physics, University of Waterloo, Waterloo, Ontario, Canada N2L 3G1*
[2]*T4, Theoretical Division, MS B213, Los Alamos National Laboratory, Los Alamos, New Mexico, 87545, USA*
[3]*Department of Physics, The College of Wooster, Wooster, Ohio, 44691, USA*
[4]*Perimeter Institute for Theoretical Physics, Waterloo, Ontario, Canada N2J 2W9*

(Received 13 August 2008; published 8 January 2009)

We use NMR quantum simulators to study antiferromagnetic Ising spin chains undergoing quantum phase transitions. Taking advantage of the sensitivity of the systems near criticality, we detect the critical points of the transitions using a direct measurement of the Loschmidt echo. We test our simulators for spin chains of even and odd numbers of spins, and compare the experimental results to theoretical predictions.

DOI: 10.1103/PhysRevA.79.012305 PACS number(s): 03.67.Lx, 73.43.Nq

I. INTRODUCTION

Quantum phase transitions (QPTs) describe sudden changes of the ground state of a many-body quantum system as a nonthermal control parameter moves through some critical value [1] (at zero temperature). QPTs are relevant not only for understanding of quantum many-body systems, but also for other problems such as quantum entanglement [2] and quantum computing, e.g., adiabatic quantum computing [3] and quantum estimation [4]. Interesting phenomena related to QPTs have recently been experimentally observed in various systems, such as heavy fermions and Bose-Einstein condensates [5].

There has been a recent flurry of activity following the observation [6] that the proximity to a quantum critical point enhances the sensitivity of a system to external perturbations, as measured by quantum-information-theoretical quantities such as the Loschmidt echo [6] or the ground-state fidelity [7]. Exploiting such sensitivity, one can detect quantum criticality by coupling an additional spin as a probe to the system undergoing a QPT. This was suggested in [8] and demonstrated in [9], where the local coupling to the probe qubit was used as the perturbation.

Here, we implement an alternative method to detect the critical point of a QPT by measuring an arbitrary qubit of the quantum critical system while applying a global perturbation. The critical parameters of a general QPT, i.e., including critical points and exponents, can in principle be detected using our method. Our approach does not require an additional probe spin, which makes the experimental implementation easier. In contrast to our method, in the previous approach [9] the efficiency of detection depended on the nature of the phases on both sides of the critical points, and could be affected, or even rendered insensitive, by the locality of the probe. Furthermore, because our method uses a global perturbation, it increases the echo signal, making it, in principle, better suited for scalability with the size of the system.

The paper is organized as follows: In Sec. II we introduce the model and discuss how we use it to simulate a second-order QPT. In Sec. III we review the behavior of the Loschmidt echo in a critical system using a perturbative treatment. In particular, we discuss the echo decay rate and its scaling near the critical point. In Sec. IV we describe the experimental implementation for even and odd spin chains using nuclear magnetic resonance, and compare our results to theoretical expectations. We offer concluding remarks in Sec. V.

II. ISING CHAIN WITH A TILTED FIELD

To demonstrate the detection of quantum criticality, we simulate the QPTs using a one-dimensional antiferromagnetic Ising model with the Hamiltonian

$$H = \sum_{i=1}^{N-1} \sigma_z^i \sigma_z^{i+1} + B_z \sum_{i=1}^{N} \sigma_z^i + B_x \sum_{i=1}^{N} \sigma_x^i, \tag{1}$$

where B_z and B_x denote longitudinal and transverse magnetic fields, respectively, σ_z^i and σ_x^i are Pauli matrices acting on spin i of the chain, and the coupling strength has been set to unity. This type of model has been extensively studied in the literature in the contexts of statistical physics [10], quantum computing [11], quantum chaos [12], and QPTs [13–22].

Notice that the general case of Eq. (1) with $B_z \neq 0$ and $B_x \neq 0$ cannot be solved exactly using Jordan-Wigner transformation methods because the longitudinal field maps into high-order coupling of the resulting fermions. This can also be seen by noting that the Hamiltonian (1) can be mapped into a classical two-dimensional (2D) Ising model [23], with

---

[*] Corresponding author: j87zhang@iqc.ca; zhangjfu2000@yahoo.com

[†] Corresponding author: fernando@cucchietti.com

[‡] Corresponding author: laflamme@iqc.ca

1050-2947/2009/79(1)/012305(12)

©2009 The American Physical Society

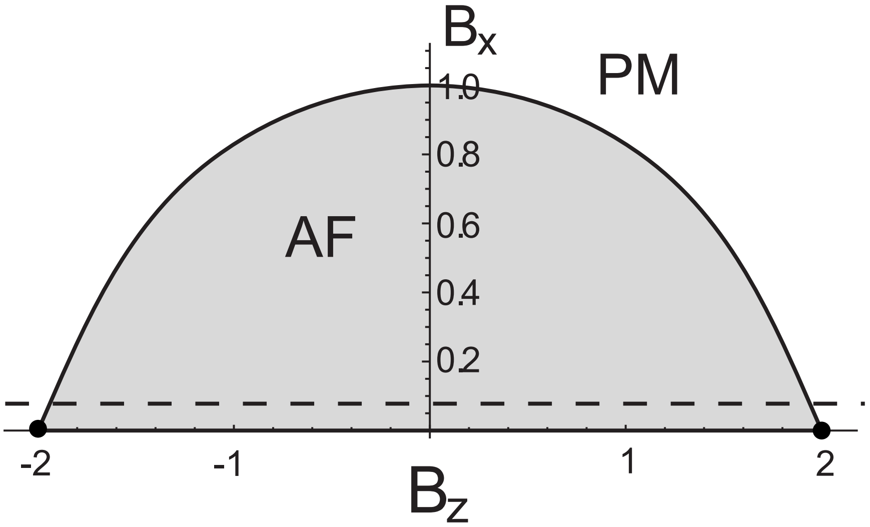

FIG. 1. Phase diagram of the antiferromagnetic Ising chain with transverse and longitudinal fields, B_x and B_z, respectively, in the thermodynamic limit of infinite chain size [22,24]. The coupling strength is chosen as the unit for B_x and B_z [see Eq. (1) in the text]. In the shadowed region inside the circle the ground state is (doubly degenerate) antiferromagnetic (AF), and in the clear region outside it the ground state is paramagnetic (PM). The transition line between both phases is a second-order critical line, while the points at $B_x=0$ are first-order transitions. The phase diagram corresponds to that of a two-dimensional classic Ising model with field equal to B_z and effective temperature proportional to B_x. The dashed line shows qualitatively the region we explore experimentally, where the critical points in the thermodynamical limit are close to $B_z=\pm 2$. For the finite systems used in our experiments, we need to consider boundary effects, which show up like extra subphases inside the AF phase. For odd N, a new critical point appears at $B_z=0$, while for even N two extra critical points appear at $B_z=\pm 1$.

B_z the longitudinal field and B_x an effective temperature, which means that our quantum simulation can also be seen as a simulation of this archetypal model of classical phase transitions. The map between a quantum d-dimensional spin system into a $d+1$ classical Ising system [23] lets us obtain the phase diagram of Hamiltonian (1) in the thermodynamic limit, which corresponds to that of the 2D classical antiferromagnetic Ising model [24], and is shown qualitatively in Fig. 1. The critical line is second order except for $B_x=0$, where it is a first-order transition. As we will use only a few qubits, we are concerned here only with finite systems. Furthermore, the Loschmidt echo decay rate typically increases with system size [8], which implies that in the thermodynamic limit the echo would decay infinitely fast (unless the perturbation is simultaneously reduced to zero, where a singular decay rate would be obtained [8]). In the finite-size systems under consideration, the gap across a second-order transition never closes, but rather reaches a minimum near the critical point (this minimum goes to zero in the thermodynamic limit). Furthermore, for finite systems we need to consider odd-even effects, which in our model system will introduce "quasi"-phases that come from boundary effects and merge in the thermodynamic limit.

Let us consider first the ground states for $B_x=0$, which will be relevant for our experiments. We keep in mind that in this particular case the system undergoes crossovers as a function of B_z, since only the energies, not the eigenstates, depend on B_z. When N is an odd integer, the ground state of the system is

$$|\psi^o(B_z)\rangle = \begin{cases} |\underbrace{00\ldots0}_{N}\rangle & (B_z < -2) \\ |\underbrace{01\ldots01}_{(N-1)/2 \text{ pairs of } 01}\;0\rangle & (-2 < B_z < 0) \\ |\underbrace{10\ldots10}_{(N-1)/2 \text{ pairs of } 10}\;1\rangle & (0 < B_z < 2) \\ |\underbrace{11\ldots1}_{N}\rangle & (B_z > 2), \end{cases} \tag{2}$$

where $|0\rangle$ and $|1\rangle$ are the eigenstates of σ_z. We denote the four phases of the ground state as $|\psi_k^o\rangle$ with $k=1,\ldots,4$. The energy of the ground state is

$$E_g^o(B_z) = \begin{cases} N\left(B_z + \dfrac{N-1}{N}\right) & (B_z \leqslant -2) \\ N\left(\dfrac{B_z}{N} - \dfrac{N-1}{N}\right) & (-2 \leqslant B_z \leqslant 0) \\ N\left(-\dfrac{B_z}{N} - \dfrac{N-1}{N}\right) & (0 \leqslant B_z \leqslant 2) \\ N\left(-B_z + \dfrac{N-1}{N}\right) & (B_z \geqslant 2). \end{cases} \tag{3}$$

We denote the energy corresponding to the four phases $|\psi_k^o\rangle$ as $E_{g,k}^o$, respectively. $B_z=B_c=\pm 2$ and 0 are the crossover points, where the system has a degenerate ground state.

$(N+1)/2$ degenerate states exist at $B_c=\pm 2$, making them the multiphase points of the system [15,25].

When N is an even integer larger than 2, the ground state of the system is

$$|\psi^e(B_z)\rangle=\begin{cases}|\underbrace{00\ldots0}_{N}\rangle & (B_z<-2)\\ \frac{1}{\sqrt{2}}[|\underbrace{01\ldots01}_{(N-2)/2\text{ pairs of }01}00\rangle+|00\underbrace{10\ldots10}_{(N-2)/2\text{ pairs of }10}\rangle] & (-2<B_z<-1)\\ \frac{1}{\sqrt{2}}[|\underbrace{01\ldots01}_{N/2\text{ pairs of }01}\rangle+|\underbrace{10\ldots10}_{N/2\text{ pairs of }10}\rangle] & (-1<B_z<1)\\ \frac{1}{\sqrt{2}}[|11\underbrace{01\ldots01}_{(N-2)/2\text{ pairs of }01}\rangle+|\underbrace{10\ldots10}_{(N-2)/2\text{ pairs of }10}11\rangle] & (1<B_z<2)\\ |\underbrace{11\ldots1}_{N}\rangle & (B_z>2),\end{cases} \tag{4}$$

and the energy of the ground state is

$$E_g^e(B_z)=\begin{cases}N\left(B_z+\frac{N-1}{N}\right) & (B_z\leqslant -2)\\ N\left(\frac{2B_z}{N}-\frac{N-3}{N}\right) & (-2\leqslant B_z\leqslant -1)\\ N\left(-1+\frac{1}{N}\right) & (-1\leqslant B_z\leqslant 1)\\ N\left(-\frac{2B_z}{N}-\frac{N-3}{N}\right) & (1\leqslant B_z\leqslant 2)\\ N\left(-B_z+\frac{N-1}{N}\right) & (B_z\geqslant 2).\end{cases} \tag{5}$$

The crossover points are $B_c=\pm 2$ and $B_c=\pm 1$. Points $B_c=\pm 2$ are also multiphase points, each with $N/2$ degenerate states. The five phases are denoted as $|\psi_k^e\rangle$ with $k=1,\ldots,5$ and the corresponding energy is represented as $E^e_{g,k}$.

From Eqs. (3) and (5), one finds that if $N\to\infty$, $E^o_{g,2}\to E^o_{g,3}$, $E^e_{g,2}\to E^e_{g,3}$, and $E^e_{g,4}\to E^e_{g,3}$. Hence, in the thermodynamic limit only the multiphase points $B_c=\pm 2$ are the crossover points, and $|\psi_2^o\rangle$, $|\psi_3^o\rangle$, $|\psi_2^e\rangle$, $|\psi_3^e\rangle$, and $|\psi_4^e\rangle$ are quasiphases that merge into a single antiferromagnetic phase (see Fig. 1). The finite-size energy phase diagrams are shown in Figs. 2(a) and 2(b).

In general, second-order QPTs are characterized by a closing of the gap between the ground and first excited energy levels at the critical points (in the thermodynamic limit). Using our small quantum information processors, we will simulate the evolution of the quantum system described by Hamiltonian (1) in a regime where its spectrum is similar to the general case of a finite-size second-order QPT (that is, with a small but finite gap). We achieve this by using a small transverse field B_x to lift the degeneracy at points B_c, which makes the spectra resemble a continuous QPT [26]. Thus, we explore the transitions crossed by the dashed line in Fig. 1. In the analysis of our results we must take into consideration finite-size effects such as the size of the gap at the critical points, and the additional quasiphases introduced by flipping a finite number of spins at the ends of the chain, which makes a distinction between experiments with odd and even chains.

III. LOSCHMIDT ECHO AND QUANTUM PHASE TRANSITIONS

A. Detection of critical parameters

Let us consider a system with Hamiltonian H_0, controlled by an external parameter λ (in our experiments, λ is the longitudinal field B_z). We assume H_0 to have gapped phases around a critical point λ_c, and without loss of generality we write a perturbed system Hamiltonian $H_1=H_0+\varepsilon V$, where V is an arbitrary Hermitian operator (to be defined later) and ε is the strength of the perturbation. Taking the ground state $|0(\lambda)\rangle$ of H_0 as the initial state, the time dependent Loschmidt echo [27] takes the form

$$L(t)\equiv|\ell(t)|^2=|\langle 0(\lambda)|e^{iH_1t}e^{-iH_0t}|0(\lambda)\rangle|^2. \tag{6}$$

Notice that the evolution under H_0 gives a physically irrelevant phase, which we keep for convenience of notation. The correspondence of the quantum critical points, a QPT, and the minima of the Loschmidt echo for *long times* has been shown for many systems [6,28]. However, the dynamical behavior for short times depends on the symmetries of the phases around the critical point and those of the perturbation operator. For instance, a monotonic increase of the decay rate with a singularity in its first derivative has been observed for some systems with local perturbations [28]. On the other hand, in the experimental results shown in the next section we observe that, for a fixed short time, the Loschmidt echo approaches a minima in the vicinities of the critical points. In this section we are concerned with providing a theoretical framework to these experimental observations. For this, we will analyze the Loschmidt echo for short times using a perturbative approach (similar to the one of Ref. [28]), and particularize to the universality of the system we simulate in the experiments.

For small perturbations ε we expand the echo amplitude

$$\ell(t) \simeq \ell(t)\big|_{\varepsilon=0} + \left.\frac{\partial \ell(t)}{\partial \varepsilon}\right|_{\varepsilon=0} \varepsilon + \left.\frac{\partial^2 \ell(t)}{\partial \varepsilon^2}\right|_{\varepsilon=0} \frac{\varepsilon^2}{2}. \tag{7}$$

The first term is

$$\ell(t)\big|_{\varepsilon=0} = \langle 0(\lambda)| e^{iH_0 t} e^{-iH_0 t} |0(\lambda)\rangle = 1. \tag{8}$$

For the second and third terms, we need to compute derivatives of the perturbed evolution operator. We can do this by expanding into infinite series and resumming after computing the expectation value of the operators in the ground state. After some algebra (see the Appendix), we find

$$\left.\frac{\partial \ell(t)}{\partial \varepsilon}\right|_{\varepsilon=0} = (-it)V_{00}, \tag{9}$$

$$\left.\frac{\partial^2 \ell(t)}{\partial \varepsilon^2}\right|_{\varepsilon=0} = 2\sum_{\alpha=0}^{N-1} |V_{0\alpha}|^2 \times \frac{e^{-i(E_\alpha - E_0)t} - 1 + it(E_\alpha - E_0)}{(E_\alpha - E_0)^2}, \tag{10}$$

where α indexes the N eigenstates of H_0 with energy E_α, E_0 is the ground-state energy, and $V_{0\alpha}=\langle \alpha(\lambda)|V|0(\lambda)\rangle$. The second-order term of Eq. (10) resembles the so-called fidelity susceptibility [29] and the quantum geometric tensor [30] that have been shown to display singular behavior and scaling near a critical point. Indeed, if we take the Fourier transform of $|L(t)|^2$, we obtain the fidelity susceptibility [29] for low frequencies. Higher frequency components appear that are related to the extra terms in the local density of states that generalizes the ground-state fidelity [6].

Our final perturbative expression for the Loschmidt echo is then

$$L(t) \simeq 1 - 2\varepsilon^2 \sum_{\alpha=1}^{N-1} |V_{0\alpha}|^2 \frac{1 - \cos(E_\alpha - E_0)t}{(E_\alpha - E_0)^2}. \tag{11}$$

B. Landau-Zener QPT toy model

When the main contribution to the sum in Eq. (11) is given by the first excited state, we can approximate

$$L(t) \simeq 1 - 2\frac{|V_{01}|^2}{\Delta^2}\varepsilon^2(1 - \cos \Delta t), \tag{12}$$

where $\Delta = E_1 - E_0$ is the gap that has a minimum at the critical point, and we have assumed that there are no degeneracies. For degenerate systems like our experimental one, we just have to replace $|V_{01}|^2$ by a sum over the degenerate subspace of the transition elements squared. In a typical second-order QPT, $\Delta \sim |\lambda - \lambda_c|^{-z\nu}$, where ν is the correlation length critical exponent and z is the dynamical critical exponent. As described in Sec. II, for a finite system the gap does not close but reaches a minimum Δ_{min} that goes to zero with the size of the system N. Thus, nonanalyticities occur only in the thermodynamic limit $N \to \infty$.

Equation (12) suggests that whenever the ground and first excited states are the most relevant for a particular system dynamics, we can study the qualitative features of a QPT with a two-level toy system under both transversal and longitudinal fields,

$$H_{LZ} = \Delta_{min}\sigma_x + s(\lambda)|\lambda|^{z\nu}\sigma_z, \tag{13}$$

where $s(\lambda)$ is the sign function. Furthermore, this toy model—which represents Eq. (12) exactly up to $O(\varepsilon^2)$—resembles the approximations we use to model a QPT with our NMR quantum simulator [see Fig. 2 for a comparison between exact results and this approximation].

From the spectra of our numerical simulations (see Fig. 2), we see that our experiments are best described by $z\nu=1$. In this case, Eq. (13) is the well-known Landau-Zener model [31] that has been used successfully to predict the scaling laws for the creation of topological defects when a system is quenched at finite speed through a critical point [32]. For this Landau-Zener model,

$$\Delta = 2\sqrt{\lambda^2 + \Delta_{min}^2}, \tag{14}$$

$$|V_{01}|^2 = \frac{\Delta_{min}^2}{\Delta_{min}^2 + \lambda^2}, \tag{15}$$

which means it has a "critical point" at $\lambda=0$. Expanding Eq. (12) for short times, and replacing with Eq. (15),

$$L(t) \simeq \exp\left(-\frac{\varepsilon^2 \Delta_{min}^2 t^2}{\Delta_{min}^2 + \lambda^2}\right). \tag{16}$$

Since the decay rate of $L(t)$ (proportional to $|V_{01}|^2$) has its maximum at $\lambda=\lambda_c=0$, then we conclude that the decay of the echo is strongest at the critical point—or, conversely, that for a fixed time t the echo has a minimum at the critical point.

In order to discuss possible universal scaling properties of the Loschmidt echo, our generalization in Eq. (13) from a Landau-Zener model attempts to incorporate a gap that closes with an arbitrary power $z\nu \neq 1$. In this general case the short-time decay is still given by Eq. (16), with a decay rate $\varepsilon^2|V_{01}|^2$. By choosing $V=\sigma_z$ independent of λ and ε, and taking $\Delta_{min}=1/N$ for demonstrative purposes, we find that near the critical point,

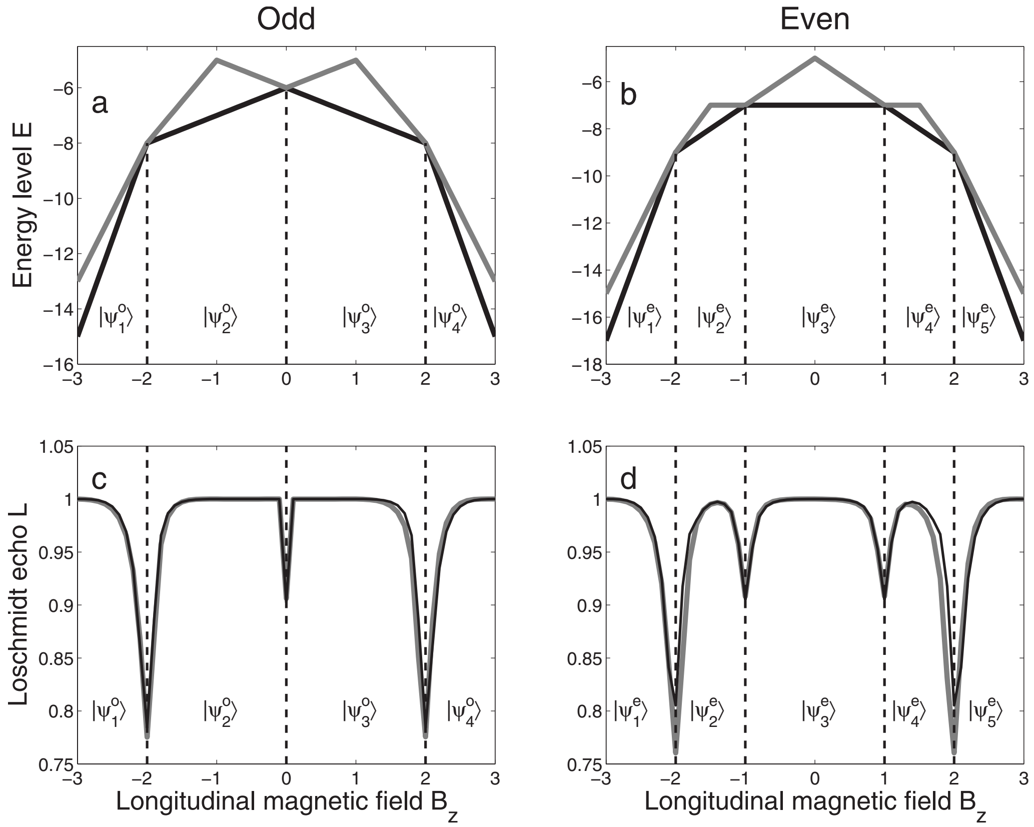

FIG. 2. Phase diagrams without transverse field [(a) and (b)] and Loschmidt echo (dimensionless) with small transverse field [(c) and (d)] for the Ising chains with odd and even spins, shown in the left and right columns, respectively. The dark and light curves in (a) and (b) represent the two lowest energy levels, by setting the coupling strength and $\hbar$ to unity. The phases and energy levels are listed in Eqs. (2)–(5). The crossover points are $B_c = \pm 2, 0$ in the odd spin system, and $B_c = \pm 2, \pm 1$ in the even spin system. The minima of the Loschmidt echo in (c) and (d) indicated the critical points. Without loss of generality, we choose $N=7$ and 8 to illustrate the odd and even cases, where $\varepsilon = 0.1$, $\tau = \pi$, and $B_x = 0.1$, for calculating L. In (c) and (d) the light thick curves show the numerical results from Eq. (6), while the dark thin curves show the approximate analytical results from Eq. (12).

$$|V_{01}|^2 N \rightarrow \infty \sim \frac{1}{N^2|\lambda - \lambda_c|^{2z\nu}}. \tag{17}$$

This suggests that the decay rate of the Loschmidt echo might show scaling with universal exponents. Such scaling has been proven for the ground-state fidelity and the quantum geometric tensor [30]. In principle, our experimental technique could be used to test universality and scaling properties of the system. However, our experiments are currently limited to the case $z\nu = 1$ and relatively small sizes that prevent us from exploring these properties.

IV. NMR IMPLEMENTATION

A. Overview of the experiment

Our goal is to measure the Loschmidt echo in the antiferromagnetic spin chain described by Hamiltonian (1) as a parameter (B_z) is varied, and from this infer the critical points of the system. Step by step, the experiment can be summarized as follows: Starting from the thermal equilibrium state, we prepared a pseudopure state (gate sequences for this are shown in Figs. 3 and 7). For each value B_z we transform the pseudopure state from the computational basis to the ground state of the Hamiltonian (1) (that depends on B_z) using a unitary U_0. We evolved the system forward in time with the Hamiltonian (1) at field B_z, and then backwards with a per-

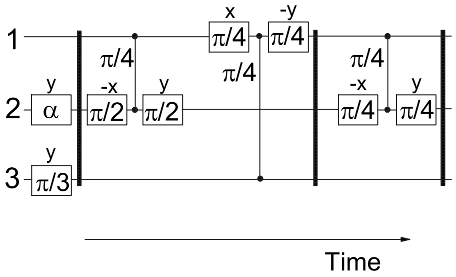

FIG. 3. Gate sequence to prepare the effective pure state $|000\rangle$ by spatial averaging from the thermal equilibrium state of TCE, where $\cos\alpha = 2\gamma_C/\gamma_H$. Here γ_H and γ_C denote the gyromagnetic ratios of proton and carbon, respectively. The single-qubit gates are implemented through radio frequency pulses denoted by the rectangles. The rotation angles and directions are shown inside and above the rectangles. The bold vertical lines denote the gradient pulses along the z-axis. The two filled circles connected by a line denote the J-coupling evolution $e^{-i\phi\sigma_z^l\sigma_z^k}$ between qubits l and k, where ϕ is shown next to the line.

turbed field $B_z+\varepsilon$. After transforming the state back to the computational basis using $U_0^\dagger$, we encode L as the diagonal element that is indicated by the initial computational basis in the density matrix. Exploiting another operation D to eliminate the nondiagonal elements of the density matrix, we can obtain the locations of the minima of L using a selective readout pulse and observing the intensity of a spectrum of a single qubit. We perform the experiment in chains of three and four spins. The results are shown in Figs. 6 and 10, respectively.

We simplify the implementation of the experiment with a number of approximations summarized here and described in detail in the following sections. At each value of B_z we prepare a very good approximation of the ground state, with fidelity higher than 98% (we elaborate on this point in the Conclusions). The approximated ground state is obtained with perturbation theory around the crossover point of the zero transverse field and does not require knowledge of the criticality of the system with the nonzero transverse field. We split the range of the field B_z in intervals (three and four for the odd and even spin chains, respectively) and use a different pulse sequence for each interval. The forward-backward evolution is compressed into a single step using a first-order Trotter expansion with 98% accuracy. The quantum networks for the odd and even chain experiments are shown in Figs. 4 and 8.

B. Efficient detection of critical points using the Loschmidt echo

In order to measure the Loschmidt echo we first prepare the ground state $|\psi(B_z,B_x)\rangle$ of $H(B_z,B_x)$, which remains very close to Eqs. (2) and (4), except in the vicinity of the critical points. Then, we evolve it forward under H for a period of time t, and next evolve it backwards under $H+\varepsilon V$ for t, where εV is the fixed perturbation introduced for detection with $|\varepsilon|\ll 1$. Here, B_z will be our control parameter (λ in the previous section), and we choose the perturbation as $V=-\Sigma_{i=1}^{N}\sigma_z^i$. This choice of a global perturbation simplifies our experiments, although more general choices such as local perturbations lead to the same results but with a reduced signal [28]. In order to detect the critical point of the transition we fix the evolution time $t=\tau$ and the transversal field B_x, and measure L as a function of B_z [6,8]. As shown in the previous section, the critical points will be marked by the minima of

$$L \equiv L(B_z)|_{t=\tau} = |\langle\psi(B_z,B_x)|U_p^\dagger U|\psi(B_z,B_x)\rangle|^2, \qquad (18)$$

where $U=e^{-i\tau H}$ and $U_p=e^{-i\tau(H+\varepsilon V)}$ are the unperturbed and perturbed evolution operators, respectively. We show some representative echoes in small chains in Figs. 2(c) and 2(d).

Measuring an overlap such as Eq. (18) in general might require full state tomography techniques. Because of its particular form, we can also couple the system to a probe qubit in such a way that L is encoded in the off-diagonal terms of the reduced density matrix of the probe [8,9]. Here, we present a method to measure L directly in the system. We call U_0 the unitary operation that prepares $|\psi_g(B_z,B_x)\rangle$ from an arbitrary computation basis state $|s\rangle$. This is not necessarily an efficient operation for all systems—indeed, finding the ground state of arbitrary Hamiltonians might be an NP-hard problem, where NP stands for nondeterministic polynomial-time [33]. However, theoretical results suggest that any initial state with a large overlap with the ground state is sufficient to detect criticality [34]. For instance, in our experiments we do not prepare the true ground state of the system, but actually a state that approximates it very well. We will discuss this and other alternatives to the preparation of the ground state in the last section.

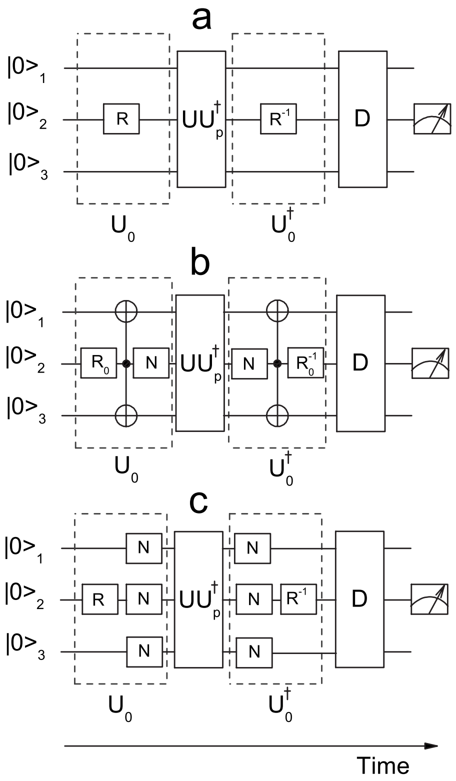

FIG. 4. Quantum networks for measuring critical points in intervals $B_z\in[-3,-1]$, $(-1,1)$, and $[1, 3]$ in the three-qubit system, shown in (a)–(c), respectively. $R=e^{i\varphi\sigma_y}$, where φ is given by Eq. (22), and $R_0=\mathbf{1}$ (unit operator), $e^{i\pi\sigma_y/4}$ or $e^{i\pi\sigma_y/2}$ for $B_z=-0.5$, 0, or 0.5, respectively. U_0 and $U_0^\dagger$ are indicated by the dashed rectangles, and $U_p^\dagger U\approx e^{-i\tau\varepsilon(\sigma_z^1+\sigma_z^2+\sigma_z^3)}$. ⊕ and the black dot connected by a line denote a controlled-NOT gate, and N denotes a NOT gate. D denotes the operation to eliminate the nondiagonal elements of the density matrix. The last operation in each figure denotes the measurement, which can be applied to an arbitrary qubit of the system.

Through rewriting Eq. (18) as

$$L = |\langle s|U_0^\dagger U_p^\dagger U U_0|s\rangle|^2, \qquad (19)$$

we find that L can be obtained by projecting

$$|\Psi\rangle = U_0^\dagger U_p^\dagger U U_0|s\rangle \qquad (20)$$

onto state $|s\rangle$, i.e., L is equal to the element $|s\rangle\langle s|$ of the density matrix $\rho=|\Psi\rangle\langle\Psi|$. Without loss of generality, we chose $|s\rangle=|00\ldots0\rangle$, the state with all qubits in computational basis state $|0\rangle$. After the final evolution $U_0^\dagger$, we eliminate the nondiagonal elements by gradient pulses or dephasing processes [35,36]. Then, through a readout pulse, e.g., $\pi/2$, applied to an arbitrary qubit, we obtain the signals marked by the states of other qubits.

We are only concerned with the signal marked by the state in which all other qubits are in state $|0\rangle$. Because in NMR we observe differences in populations, the amplitude of this signal A is proportional to $(L-\rho_{nn})\leqslant L$, with $n\neq 1$. The locations of the minima of A are the same as those of L, with their values each decreased by an additional ρ_{nn}. This allows us to detect the critical points through A by measuring only one qubit of the system.

C. Odd N case

We first demonstrate the detection of critical points of a QPT in an odd spin system with $N=3$. We prepared an initial state that approximates the ground state of the Hamiltonian for each value of B_z. Using our notation for the ground states of H for $B_x=0$ ($|\psi_k^o\rangle=|000\rangle$, $|010\rangle$, $|101\rangle$, and $|111\rangle$, for $k=1\ldots4$, respectively), the ground state near $B_c=\pm2$ can be approximated as

$$|\psi(B_z,B_x)\rangle=|\psi_m^o\rangle\cos\varphi-|\psi_n^o\rangle\sin\varphi, \tag{21}$$

with

$$\tan\varphi=[(2-|B_z|)+\sqrt{(2-|B_z|)^2+B_x^2}]/B_x, \tag{22}$$

where $m=1$, $n=2$ or $m=4$, $n=3$, corresponding to $B_c=-2$ or 2, respectively. In the vicinity of $B_c=0$, the gap between the lowest energy levels is so small that the ground state can be well approximated by $|\psi_2^o\rangle$, $(|\psi_2^o\rangle-|\psi_3^o\rangle)/\sqrt{2}$, or $|\psi_3^o\rangle$, corresponding to $B_z<0$, $B_z=0$, or $B_z>0$, respectively.

For the experimental implementation, we used ^{13}C labeled trichloroethylene (TCE), dissolved in d-chloroform as the sample [37]. Data were taken with a Bruker DRX 700 MHz spectrometer. We denote the ^{1}H nuclear spin as qubit 2 (H2), the ^{13}C directly connected to ^{1}H is denoted as qubit 1 (C1), and the other ^{13}C as qubit 3 (C3). The difference of frequency between C1 and C3 is about 1249.2 Hz, and the coupling constants are $J_{13}=103.1$ Hz, $J_{12}=200.9$ Hz, and $J_{23}=9.16$ Hz. The spin-selective excitation for C1 or C3 is realized by a GRAPE pulse, where GRAPE stands for gradient ascent pulse engineering [38]. The J-coupling evolution $e^{-i\phi\sigma_z^l\sigma_z^k}$ between qubits l and k is implemented by a standard refocusing pulse sequence [39]. The effective pure state $|000\rangle$ is prepared by spatial averaging [40] from the thermal equilibrium state $\rho_{eq}=\gamma_{\mathrm{H}}\sigma_z^2+\gamma_{\mathrm{C}}(\sigma_z^1+\sigma_z^3)$, by approximating the system as a weakly coupling system, where γ_{H} and γ_{C} denote the gyromagnetic ratios of proton and carbon, respectively. The gate sequence for the pseudo-pure state preparation is shown as Fig. 3.

In order to measure the echo we split the B_z axis in intervals near $B_c=-2$, 0, and 2. In particular, we use different quantum networks for $B_z\in[-3,-1]$, $(-1,1)$, and $[1,3]$, shown in Figs. 4(a)–4(c), respectively. The operations for preparing U_0 and $U_0^\dagger$ are indicated by the dashed rectangles and D denotes the operation to eliminate the nondiagonal elements of the density matrix. Figure 5 shows the corresponding gate sequences. The evolution time is chosen as $\tau=\pi$, and $\varepsilon=0.2$ or 0.125. The echo evolution $U_p^\dagger U$ can be approximated by $U_p^\dagger U\approx e^{-i\tau\varepsilon(\sigma_z^1+\sigma_z^2+\sigma_z^3)}$ with fidelity larger than 98%. We optimize the gate sequence $\mathrm{CNOT}_{21}-e^{-i\tau\varepsilon\sigma_z^1}-\mathrm{CNOT}_{21}$ as $e^{-i\tau\varepsilon\sigma_z^1\sigma_z^2}$, and $\mathrm{CNOT}_{23}-e^{-i\tau\varepsilon\sigma_z^3}-\mathrm{CNOT}_{23}$ as $e^{-i\tau\varepsilon\sigma_z^2\sigma_z^3}$ (where CNOT stands for controlled-NOT) [41] to obtain Fig. 5(b) from Fig. 4(b). The amplitudes of signals are obtained by measuring on H2, with experimental results shown in Fig. 6. Experimental data are marked by "×" and "+" for $\varepsilon=0.2$ and $\varepsilon=0.125$, respectively. The corresponding theoretical results are indicated by the light and dark curves. The critical points are correctly indicated by the minima of the amplitudes.

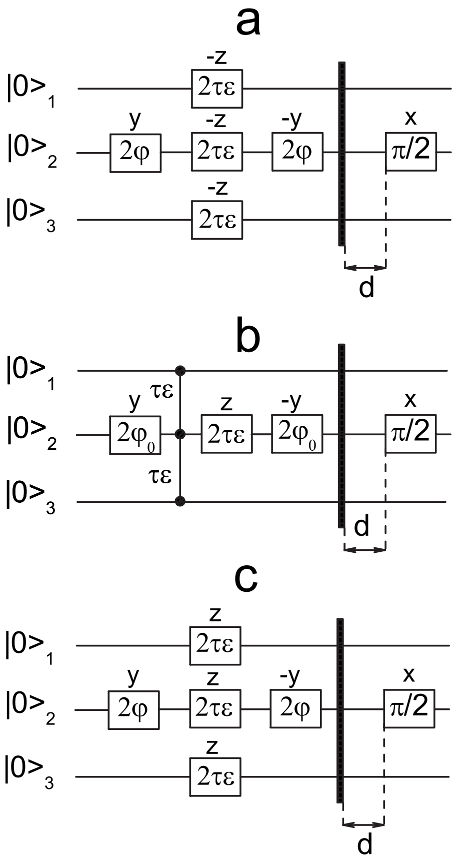

FIG. 5. Gate sequences (a)–(c) to implement Figs. 4(a)–4(c), respectively. A 16-step average over a random delay, denoted by d, between 0 and 10 ms, dephases the residual zero-quantum coherence. The last $\pi/2$ pulse is the readout pulse, which can be applied to an arbitrary qubit of the system.

D. Even N case

We illustrate the detection of QPT critical points in an even spin chain with $N=4$. Here we use the notation for the ground states for $B_x=0$, $|\psi_k^e\rangle=|0000\rangle$, $(|0100\rangle+|0010\rangle)/\sqrt{2}$, $(|0101\rangle+|1010\rangle)/\sqrt{2}$, $(|1101\rangle+|1011\rangle)/\sqrt{2}$, and $|1111\rangle$, for $k=1\ldots5$, respectively. Depending on the value of B_z we prepare an approximation to the ground state

$$\psi(B_z,B_x)=|\psi_m^e\rangle\cos\varphi-|\psi_n^e\rangle\sin\varphi. \tag{23}$$

For B_z near $B_c=\pm2$,

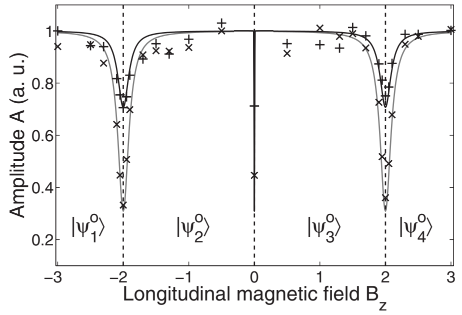

FIG. 6. Experimental results in the three-qubit QPT system, where $\tau=\pi$. The four phases $|\psi_k^o\rangle$ with $k=1,\ldots,4$ are represented as $|\psi_k^o\rangle=|000\rangle$, $|010\rangle$, $|101\rangle$, and $|111\rangle$, respectively. The experimentally measured amplitudes of the signals are marked by × and + for $\varepsilon=0.2$ and 0.125, respectively. The minima of the amplitudes indicate the critical points. The theoretical results are shown as the light and dark curves. The experimental results show a good agreement with theory.

$$\tan\varphi=[(2-|B_z|)+\sqrt{(2-|B_z|)^2+2B_x^2}]/(\sqrt{2}B_x), \qquad (24)$$

with $m=1$, $n=2$, or $m=5$, $n=4$, corresponding to $B_c=-2$ or 2, respectively. For B_z near $B_c=\pm 1$ we use

$$\tan\varphi=[(1-|B_z|)+\sqrt{(1-|B_z|)^2+B_x^2}]/B_x, \qquad (25)$$

with $m=2$, $n=3$ or $m=4$, $n=3$, corresponding to $B_c=-1$ or 1, respectively.

For implementation, we choose the four carbons in crotonic acid [42] dissolved in *d*6-acetone as the four qubits by decoupling the protons. Data were taken with a Bruker DRX 700 MHz spectrometer. The chemical shifts for the four carbons ν_{1-4} are −2965.75, −25 501.9, −21 583.9, and −29 431.5 Hz. The J couplings are $J_{12}=41.6$, $J_{23}=69.7$, $J_{34}=72.0$, $J_{13}=1.5$, $J_{14}=7.0$, and $J_{24}=1.2$ Hz.

We prepare the pseudopure state by spatial averaging through improving the scheme found in [43]. Our technique can be illustrated by transforming the thermal equilibrium state of a four-qubit system $\Sigma_{i=1}^{4}\sigma_z^i$ to

$$\left(\sum_{i=1}^{3}\sigma_z^i\right)(\mathbf{1}/2+\sigma_z^4)+\sigma_z^4/8, \qquad (26)$$

where $\mathbf{1}$ denotes the unit operator and $\Sigma_{i=1}^{3}\sigma_z^i$ can be transformed to an effective pure state in the three-qubit system. This method generalizes to an N-qubit system in a recursive manner. After some simplifications [44], the complete gate sequence to generate $|0000\rangle$ is shown in Fig. 7, where the state specific swap gate requires two J couplings with evolution time $1/(2J_{lk})$ [45]. In the ideal case the strength of the single peak obtained through a $\pi/2$ readout pulse selective for one spin is equal to that of the same peak in a spectrum of the thermal state, where eight peaks with equal strength appear.

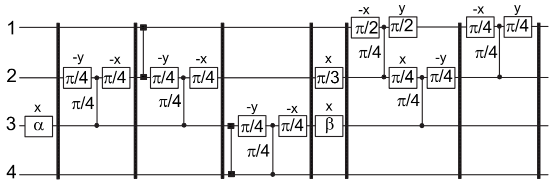

FIG. 7. Gate sequence to prepare the effective pure state $|0000\rangle$ by spatial averaging from the thermal equilibrium state of the four carbons in crotonic acid, where $\cos\alpha=1/8$ and $\cos\beta=1/4$. The filled rectangles in pairs connected by a line denote a state specific swap gate between qubits l and k, i.e., it transforms σ_z^l to σ_z^k, or σ_z^k to σ_z^l.

The ground states are prepared from Eqs. (23)–(25). As before, we split the B_z axis in intervals around the critical points of zero transverse field. The networks to measure the echo for $B_z\in[-3,-1.44]$, and $(-1.44,0]$ are shown in Figs. 8(a) and 8(b). From these one can obtain the networks for the intervals $B_z\in[1.44,3]$ and $(0,1.44)$ simply by adding NOT gates to all qubits at the end of the corresponding networks for implementing U_0. Through compiling the pulse sequence [11], we obtain the gate sequences shown as Fig. 9, where $U_p^{\dagger}U\approx e^{-i\tau\varepsilon(\sigma_z^1+\sigma_z^2+\sigma_z^3+\sigma_z^4)}$ with fidelity larger than 98% and the two SWAP gates are canceled because they commute with $e^{-i\tau\varepsilon(\sigma_z^2+\sigma_z^3)}$. Experimental results are shown in Fig. 10, with $\tau=\pi/2$. The measured amplitudes are marked by × and + for $\varepsilon=0.5$ and 0.4, respectively. The solid curves show the corresponding theoretical results. Again, the critical points are correctly indicated by the minima of the amplitudes, so the experiment results are in good agreement with theoretical expectations. The observed errors could be explained by im-

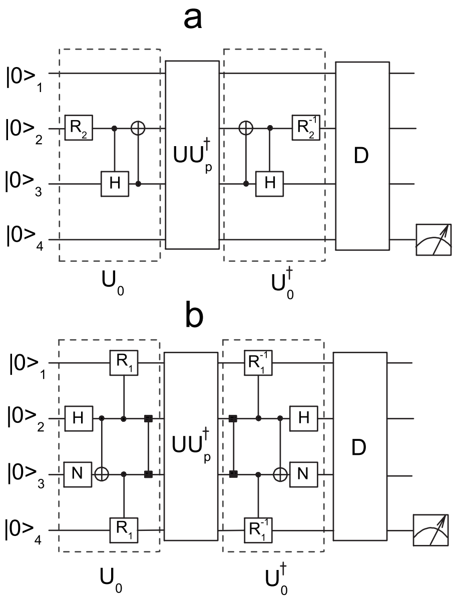

FIG. 8. Quantum network for measuring critical points in intervals $B_z\in[-3,-1.44]$ and $(-1.44,0]$ in a four-qubit system, shown in (a) and (b), respectively. H denotes the Hadamard transform gate, and $U_p^{\dagger}U\approx e^{-i\tau\varepsilon(\sigma_z^1+\sigma_z^2+\sigma_z^3+\sigma_z^4)}$. $R_2=e^{i\varphi_2\sigma_y}$ and $R_1=e^{i\varphi_1\sigma_y}$, where φ_2 and φ_1 are chosen as Eqs. (24) and (25). The rectangle and the dot connected by a line denote a controlled operation that is shown inside the rectangle. The filled rectangles in pairs connected by a line denote a SWAP gate. The networks for intervals $B_z\in[1.44,3]$ and (0, 1.44) can be obtained by adding NOT gates to all qubits at the end of the networks for implementing U_0 in (a) and (b), respectively.

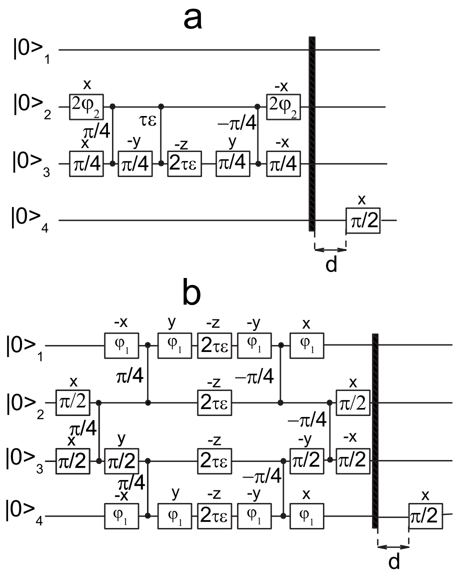

FIG. 9. Quantum gate sequences (a) and (b) to implement Figs. 8(a) and 8(b) respectively. Through replacing ε by $-\varepsilon$ in (a) and (b) one can obtain the gate sequences for the intervals $B_z \in [1.44, 3]$ and (0, 1.44), respectively.

perfections in the implementation of the radio frequency pulses, inhomogeneities of magnetic fields, and decoherence.

V. DISCUSSION AND CONCLUSIONS

We performed experimentally quantum simulations of the second-order quantum phase transitions in finite systems. In particular, we showed the QPTs and found the critical points of three- and four-spin Ising chains, representative of odd and even spin chains, respectively. The critical points are indicated by the minima of the Loschmidt echo. We showed that this echo can be realized by inducing the perturbation with an external field, and the positions of its minima (related to the critical points) can be obtained by measuring only an arbitrary qubit of the system. In the weakly and fully resolved coupling systems, the resonance lines can be assigned, and the line marked by the other qubits in $|0\rangle$ can be identified. However, in large size systems where the requirement of fully resolved coupled is not practical, or in the strongly coupled systems, e.g., liquid crystal or solid NMR systems, where the assignment of resonance lines are not possible, one cannot identify the marked line. For these cases, our method can be generalized by measuring the global polarizations of the whole system by a collective $\pi/2$ pulse (or N pulses selective for each qubit), replacing the readout pulse applied to one qubit. In the vicinities of the critical points, the loss of the polarization due to the decoherence process (e.g., gradient pulse or dephasing process) approaches the maxima. Hence the critical points will be indicated by the minima of the amplitude of the total signals of all qubits. Furthermore, this has the advantage that a global measurement is scalable with the size of the system.

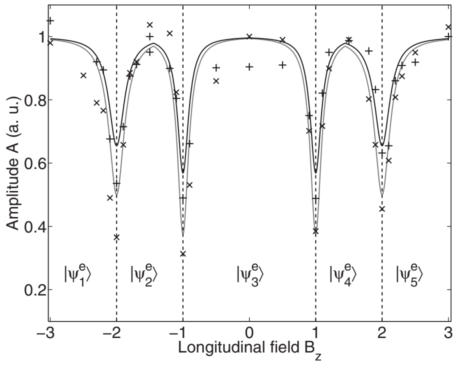

FIG. 10. Experimental results in the four-qubit QPT system, where $\tau=\pi/2$. The five phases $|\psi_k^e\rangle$ with $k=1,\ldots,5$ are represented as $|\psi_k^e\rangle=|0000\rangle$, $(|0100\rangle+|0010\rangle)/\sqrt{2}$, $(|0101\rangle+|1010\rangle)/\sqrt{2}$, $(|1101\rangle+|1011\rangle)/\sqrt{2}$, and $|1111\rangle$, respectively. The experimentally measured amplitudes are marked by × and + for $\varepsilon=0.5$ and 0.4, respectively. The minima of the amplitudes indicate the critical points. The theoretical results are shown as the light and dark curves, in good agreement with the experimental results.

Our method improves the previous one that required a probe qubit for both the perturbation and the measurement [9]. We believe this advantage gives our method better scalability with the size of the system. In particular, the perturbations created by the probe qubit method are limited by the probe-system coupling strength, and furthermore, can become weaker than the noise in large systems when they do not couple the probe to a macroscopic number of normal modes in the system. Separating the perturbation and measurement also gives finer control over the whole experiment.

On the issue of scalability, a very important point in the algorithm is the preparation of the initial state. From a theory point of view, most of the studies of the Loschmidt echo have used ground states as initial states only because of simplicity. However, preparing the ground state of an arbitrary Hamiltonian is an NP-hard problem [33]. Furthermore, it would be redundant, since it is most likely that knowing the exact ground states is equivalent to knowing everything about the system—including the information about criticality that one wants to obtain from the echo experiments. Nonetheless, there is evidence that the initial state need not be the exact ground state, but any state with a sizable overlap with the ground state. For instance, analytical studies show that thermal states at temperatures at or below the energy scales of the system can be used effectively to detect the quantum phase transition [34], where the number of the spins can be up to 200. However, in some systems (like our liquid NMR experiments) preparing a thermal state is not particularly easier than other—perhaps more useful—states. For instance, in our experiments we prepared a good approximation to the ground state that we obtained from a simple perturbation theory around the crossover point of zero transverse field. This method suggests that other approximations, such as mean field or numerical classical algorithms, could work well to detect criticality.

While the problem of finding strict minimum requirements for the initial state of the algorithm is clearly in need of more research, we feel that it is reasonable to argue that initialization of the algorithm is scalable: it only requires finding among many possibilities one that can be prepared efficiently in a quantum computer. It would be interesting to study the effect of more efficiently prepared ground states [33] or to investigate if state-independent indicators—such as the operator fidelity susceptibility proposed in Ref. [46]—could get rid of the initial state issue altogether. Finally, we would like to mention that other possible extensions of our experimental methods are using the Loschmidt echo to measure QPTs in gapless systems [46,47], and also for measuring thermal phase transitions [29,48].

ACKNOWLEDGMENTS

We thank D. Suter, J. P. Paz, C. Batista, G. Ortiz, T.-C. Wei, M. Zwolak, and H. T. Quan for helpful discussions. F.M.C. acknowledges support from DOE-LDRD programs. J.K.G. acknowledges support from the NSF-REU and Los Alamos Summer School programs.

APPENDIX: PERTURBATIVE EXPANSION OF THE LOSCHMIDT ECHO

We start from the expansion of Eq. (7),

$$\ell(t) \simeq \ell(t)|_{\varepsilon=0} + \left.\frac{\partial \ell(t)}{\partial \varepsilon}\right|_{\varepsilon=0} \varepsilon + \left.\frac{\partial^2 \ell(t)}{\partial \varepsilon^2}\right|_{\varepsilon=0} \frac{\varepsilon^2}{2}, \quad \text{(A1)}$$

where

$$\ell(t) = \langle 0(\lambda)| e^{iH_0 t} e^{-i(H_0+\varepsilon V)t} |0(\lambda)\rangle, \quad \text{(A2)}$$

with $|0(\lambda)\rangle$ the ground state of H_0, and we keep the harmless $e^{iH_0 t}$ operator because it will simplify the results. The first term of the expansion can be simply evaluated as in Eq. (8),

$$\ell(t)|_{\varepsilon=0} = \langle 0(\lambda)| e^{iH_0 t} e^{-iH_0 t} |0(\lambda)\rangle = 1. \quad \text{(A3)}$$

For the first- and second-order terms we must compute derivatives of the evolution operator. We can do this by expanding the exponential into an infinite series sum,

$$\begin{aligned}
\left.\frac{\partial \ell(t)}{\partial \varepsilon}\right|_{\varepsilon=0} &= \langle 0(\lambda)| e^{iH_0 t} \left.\frac{\partial e^{-i(H_0+\varepsilon V)t}}{\partial \varepsilon}\right|_{\varepsilon=0} |0(\lambda)\rangle \\
&= \langle 0(\lambda)| e^{iH_0 t} \frac{\partial}{\partial \varepsilon} \sum_{n=0}^{\infty} \left.\frac{1}{n!}[-i(H_0+\varepsilon V)t]^n \right|_{\varepsilon=0} |0(\lambda)\rangle \\
&= \langle 0(\lambda)| e^{iH_0 t} \sum_{n=1}^{\infty} \frac{(-it)^n}{n!} \sum_{k=0}^{n-1} (H_0+\varepsilon V)^k V \\
&\quad \times (H_0+\varepsilon V)^{n-1-k}|_{\varepsilon=0} |0(\lambda)\rangle \\
&= \langle 0(\lambda)| e^{iH_0 t} \sum_{n=1}^{\infty} \frac{(-it)^n}{n!} \sum_{k=0}^{n-1} H_0^k V H_0^{n-1-k} |0(\lambda)\rangle .
\end{aligned} \quad \text{(A4)}$$

Computing now the expectation value,

$$\begin{aligned}
\left.\frac{\partial \ell(t)}{\partial \varepsilon}\right|_{\varepsilon=0} &= e^{iE_0 t} \sum_{n=1}^{\infty} \frac{(-it)^n}{n!} \sum_{k=0}^{n-1} E_0^k V E_0^{n-1-k} \\
&= e^{iE_0 t} \sum_{n=1}^{\infty} \frac{(-it)^n}{n!} E_0^{n-1} n \langle g(\lambda)|V|g(\lambda)\rangle \\
&= (-it) V_{00} e^{iE_0 t} \sum_{m=0}^{\infty} \frac{(-itE_0)^m}{m!} \\
&= (-it) V_{00},
\end{aligned} \quad \text{(A5)}$$

where E_0 is the ground-state energy and $V_{00} = \langle 0(\lambda)|V|0(\lambda)\rangle$.

For the second-order term we continue derivting Eq. (A4) before the evaluation at $\varepsilon=0$,

$$\begin{aligned}
\left.\frac{\partial^2 \ell(t)}{\partial \varepsilon^2}\right|_{\varepsilon=0} &= \langle 0(\lambda)| e^{iH_0 t} \left.\frac{\partial^2 e^{-i(H_0+\varepsilon V)t}}{\partial \varepsilon^2}\right|_{\varepsilon=0} |0(\lambda)\rangle = \langle 0(\lambda)| e^{iH_0 t} \frac{\partial}{\partial \varepsilon} \sum_{n=1}^{\infty} \frac{(-it)^n}{n!} \sum_{k=0}^{n-1} (H_0+\varepsilon V)^k V (H_0+\varepsilon V)^{n-1-k}|_{\varepsilon=0} |0(\lambda)\rangle \\
&= \langle 0(\lambda)| e^{iH_0 t} \sum_{n=2}^{\infty} \frac{(-it)^n}{n!} \Bigg[\left(\sum_{k=1}^{n-1} \sum_{m=0}^{k-1} (H_0+\varepsilon V)^m V (H_0+\varepsilon V)^{k-1-m} V (H_0+\varepsilon V)^{n-1-k} \right) \\
&\quad + \left(\sum_{k=0}^{n-2} (H_0+\varepsilon V)^k V \sum_{m=0}^{n-2-k} (H_0+\varepsilon V)^m V (H_0+\varepsilon V)^{n-2-k-m} \right) \Bigg]_{\varepsilon=0} |0(\lambda)\rangle \\
&= \langle 0(\lambda)| e^{iH_0 t} \sum_{n=2}^{\infty} \frac{(-it)^n}{n!} \left[\left(\sum_{k=1}^{n-1} \sum_{m=0}^{k-1} H_0^m V H_0^{k-1-m} V H_0^{n-1-k} \right) + \left(\sum_{k=0}^{n-2} H_0^k V \sum_{m=0}^{n-2-k} H_0^m V H_0^{n-2-k-m} \right) \right] |0(\lambda)\rangle .
\end{aligned} \quad \text{(A6)}$$

By taking the expectation value on the ground state we now obtain

$$\left.\frac{\partial^2 \ell(t)}{\partial \varepsilon^2}\right|_{\varepsilon=0} = e^{iE_0 t} \sum_{n=2}^{\infty} \frac{(-it)^n}{n!} \left[\left(\sum_{k=1}^{n-1} \sum_{m=0}^{k-1} E_0^{n-1-k+m} \langle 0(\lambda)| V H_0^{k-1-m} V |0(\lambda)\rangle \right) + \left(\sum_{k=0}^{n-2} \sum_{m=0}^{n-2-k} E_0^{n-2-m} \langle 0(\lambda)| V H_0^m V |0(\lambda)\rangle \right) \right], \quad \text{(A7)}$$

replacing now $k' = k-1$ and $m' = m+k$ in the first and second sums inside the brackets,

$$\left.\frac{\partial^2\ell(t)}{\partial\varepsilon^2}\right|_{\varepsilon=0} = e^{iE_0t}\sum_{n=2}^{\infty}\frac{(-it)^n}{n!}E_0^{n-2}\left[\left(\sum_{k=0}^{n-2}\sum_{m=0}^{k}E_0^{-k+m}\langle 0(\lambda)|VH_0^{k-m}V|0(\lambda)\rangle\right)+\left(\sum_{k=0}^{n-2}\sum_{m=k}^{n-2}E_0^{-m+k}\langle 0(\lambda)|VH_0^{m-k}V|0(\lambda)\rangle\right)\right]$$

$$= e^{iE_0t}\sum_{n=2}^{\infty}\frac{(-it)^n}{n!}E_0^{n-2}\left[(n-1)\langle 0(\lambda)|V^2|0(\lambda)\rangle+\sum_{k=0}^{n-2}\sum_{m=0}^{n-2}E_0^{-|k-m|}\langle 0(\lambda)|VH_0^{|k-m|}V|0(\lambda)\rangle\right]. \tag{A8}$$

We can simplify the term inside the brackets by counting the number of times the terms with $|k-m|=0$, $|k-m|=1$, and so on are repeated. The final expression is then

$$\left.\frac{\partial^2\ell(t)}{\partial\varepsilon^2}\right|_{\varepsilon=0} = e^{iE_0t}\sum_{n=2}^{\infty}\frac{(-it)^n}{n!}E_0^{n-2}\left[2\sum_{k=0}^{n-2}E_0^{-k}(n-1-k)\langle 0(\lambda)|VH_0^kV|0(\lambda)\rangle\right]. \tag{A9}$$

We can make further progress by inserting identities $\sum_{\alpha=0}^{N-1}|\alpha\rangle\langle\alpha|$, with $|\alpha\rangle$ the basis of eigenstates of H_0 (we assume a finite Hilbert space $\alpha=0,\ldots,N-1$),

$$\left.\frac{\partial^2\ell(t)}{\partial\varepsilon^2}\right|_{\varepsilon=0} = e^{iE_0t}2\sum_{n=2}^{\infty}\frac{(-it)^n}{n!}E_0^{n-2}\left[\sum_{k=0}^{n-2}E_0^{-k}(n-1-k)\times\sum_{\alpha=0}^{N-1}|V_{0\alpha}|^2E_\alpha^k\right], \tag{A10}$$

where $V_{0\alpha}=\langle\alpha|V|0(\lambda)\rangle$. We can do the sum over k first,

$$\left.\frac{\partial^2\ell(t)}{\partial\varepsilon^2}\right|_{\varepsilon=0} = e^{iE_0t}2\sum_{n=2}^{\infty}\frac{(-it)^n}{n!}E_0^{n}\sum_{\alpha=0}^{N-1}|V_{0\alpha}|^2\frac{n-1+\left(\frac{E_\alpha}{E_0}\right)^n-n\left(\frac{E_\alpha}{E_0}\right)}{(E_\alpha-E_0)^2} \tag{A11}$$

(notice that the term with $\alpha=0$ is finite), followed by the sum over n,

$$\left.\frac{\partial^2\ell(t)}{\partial\varepsilon^2}\right|_{\varepsilon=0} = 2\sum_{\alpha=0}^{N-1}|V_{0\alpha}|^2\frac{e^{-i(E_\alpha-E_0)t}-1+it(E_\alpha-E_0)}{(E_\alpha-E_0)^2}$$

$$= -|V_{00}|^2t^2 - 2\sum_{\alpha=1}^{N-1}|V_{0\alpha}|^2\frac{1-e^{-i(E_\alpha-E_0)t}-it(E_\alpha-E_0)}{(E_\alpha-E_0)^2}. \tag{A12}$$

Now we need to put the results of Eqs. (A3), (A5), and (A12) into Eq. (A1).

$$\ell(t)\simeq 1-itV_{00}\varepsilon-\left(|V_{00}|^2t^2+2\sum_{\alpha=1}^{N-1}|V_{0\alpha}|^2\frac{1-e^{-i(E_\alpha-E_0)t}-it(E_\alpha-E_0)}{(E_\alpha-E_0)^2}\right)\frac{\varepsilon^2}{2}. \tag{A13}$$

Noting that V_{00} is real and keeping the term with lower order in ε, we obtain the expression for the Loschmidt echo as follows:

$$L(t)=|\ell(t)|^2\simeq 1-2\varepsilon^2\sum_{\alpha=1}^{N-1}|V_{0\alpha}|^2\frac{1-\cos(E_\alpha-E_0)t}{(E_\alpha-E_0)^2}. \tag{A14}$$

[1] S. Sachdev, *Quantum Phase Transitions* (Cambridge University Press, Cambridge, 2000); M. Vojta, Rep. Prog. Phys. **66**, 2069 (2003); P. Coleman and A. J. Schofield, Nature (London) **433**, 226 (2005).

[2] A. Osterloh, L. Amico, G. Falci, and R. Fazio, Nature (London) **416**, 608 (2002); T. R. de Oliveira, G. Rigolin, M. C. de Oliveira, and E. Miranda, Phys. Rev. Lett. **97**, 170401 (2006).

[3] E. Farhi *et al.*, Science **292**, 472 (2001); J. I. Latorre and R. Orús, Phys. Rev. A **69**, 062302 (2004); R. Schützhold and G. Schaller, *ibid.* **74**, 060304(R) (2006).

[4] P. Zanardi, M. G. A. Paris, and L. Campos Venuti, Phys. Rev. A **78**, 042105 (2008); C. Invernizzi, M. Korbman, L. C. Venuti, and M. G. A. Paris, *ibid.* **78**, 042106 (2008).

[5] S. Sachdev, Nat. Phys. **4**, 173 (2008); P. Gegenwart, Q. Si, and F. Steglich, *ibid.* **4**, 186 (2008); T. Giamarchi, C. Rüegg, and O. Tchernyshyov, *ibid.* **4**, 198 (2008).

[6] H. T. Quan, Z. Song, X. F. Liu, P. Zanardi, and C. P. Sun, Phys. Rev. Lett. **96**, 140604 (2006); Z.-G. Yuan, P. Zhang, and S.-S. Li, Phys. Rev. A **75**, 012102 (2007).

[7] P. Zanardi and N. Paunković, Phys. Rev. E **74**, 031123 (2006).

[8] F. M. Cucchietti, S. Fernandez-Vidal, and J. P. Paz, Phys. Rev. A **75**, 032337 (2007).

[9] J. Zhang, X. Peng, N. Rajendran, and D. Suter, Phys. Rev. Lett. **100**, 100501 (2008).

[10] J. R. Kirkwood, J. Stat. Phys. **37**, 407 (1984).

[11] M. D. Bowdrey, J. A. Jones, E. Knill, and R. Laflamme, Phys. Rev. A **72**, 032315 (2005).

[12] J. Karthik, A. Sharma, and A. Lakshminarayan, Phys. Rev. A

75, 022304 (2007).
[13] K. Uzelac, R. Jullien, and P. Pfeuty, Phys. Rev. B **22**, 436 (1980).
[14] M. A. Continentino, Phys. Rep. **239**, 179 (1994).
[15] P. Sen, Phys. Rev. E **63**, 016112 (2000).
[16] D. Gunlycke, V. M. Kendon, V. Vedral, and S. Bose, Phys. Rev. A **64**, 042302 (2001).
[17] W. H. Zurek, U. Dorner, and P. Zoller, Phys. Rev. Lett. **95**, 105701 (2005).
[18] P. Werner, K. Völkerr, M. Troyer, and S. Chakravarty, Phys. Rev. Lett. **94**, 047201 (2005).
[19] X. Peng, J. Du, and D. Suter, Phys. Rev. A **71**, 012307 (2005).
[20] S. Mostame, G. Schaller, and R. Schützhold, Phys. Rev. A **76**, 030304(R) (2007).
[21] S.-J. Gu *et al.*, Phys. Rev. B **77**, 245109 (2008).
[22] A. A. Ovchinnikov, D. V. Dmitriev, V. Ya. Krivnov, and V. O. Cheranovskii, Phys. Rev. B **68**, 214406 (2003).
[23] M. Suzuki, Prog. Theor. Phys. **56**, 1454 (1976).
[24] E. Müller-Hartmann and J. Zittartz, Z. Phys. B **27**, 261 (1977); K. Binder and D. P. Landau, Phys. Rev. B **21**, 1941 (1980).
[25] J. Vidal, R. Mosseri, and J. Dukelsky, Phys. Rev. A **69**, 054101 (2004).
[26] S. L. Sondhi, S. M. Girvin, J. P. Carini, and D. Shahar, Rev. Mod. Phys. **69**, 315 (1997).
[27] R. A. Jalabert and H. M. Pastawski, Phys. Rev. Lett. **86**, 2490 (2001); T. Gorin, T. Prosen, T. H. Seligman, and M. Žnidarič, Phys. Rep. **435**, 33 (2006).
[28] D. Rossini, T. Calarco, V. Giovannetti, S. Montangero, and R. Fazio, Phys. Rev. A **75**, 032333 (2007).
[29] W.-L. You, Y.-W. Li, and S.-J. Gu, Phys. Rev. E **76**, 022101 (2007).
[30] L. Campos Venuti and P. Zanardi, Phys. Rev. Lett. **99**, 095701 (2007).
[31] L. D. Landau and E. M. Lifshitz, *Quantum Mechanics* (Pergamon, London, 1958); C. Zener, Proc. R. Soc. London, Ser. A **137**, 696 (1932).
[32] B. Damski, Phys. Rev. Lett. **95**, 035701 (2005).
[33] D. Poulin and P. Wocjan, e-print arXiv:0809.2705v1.
[34] P. Zanardi, H. T. Quan, X. Wang, and C. P. Sun, Phys. Rev. A **75**, 032109 (2007).
[35] T. S. Mahesh and D. Suter, Phys. Rev. A **74**, 062312 (2006).
[36] A. M. Souza *et al.*, e-print arXiv:0711.1156v2, New J. Phys. (to be published).
[37] M. A. Nielsen, E. Knill, and R. Laflamme, Nature (London) **396**, 52 (1998).
[38] J. Baugh *et al.*, Phys. Can. **63**, 22 (2007); special issue on quantum information and quantum computing; N. Khaneja *et al.*, J. Magn. Reson. **172**, 296 (2005); C. A. Ryan, C. Negrevergene, M. Laforest, E. Knill, and R. Laflamme, Phys. Rev. A **78**, 012328 (2008).
[39] N. Linden, Ē. Kupče, and R. Freeman, Chem. Phys. Lett. **311**, 321 (1999); L. M. K. Vandersypen and I. L. Chuang, Rev. Mod. Phys. **76**, 1037 (2004).
[40] D. G. Cory *et al.*, Physica D **120**, 82 (1998); X. Peng *et al.*, e-print arXiv: quant-ph/0202010; J. Zhang, N. Rajendran, X. Peng, and D. Suter, Phys. Rev. A **76**, 012317 (2007).
[41] J. Zhang, G. L. Long, Z. Deng, W. Liu, and Z. Lu, Phys. Rev. A **70**, 062322 (2004).
[42] E. Knill *et al.*, Nature (London) **404**, 368 (2000); C. A. Ryan, J. Emerson, D. Poulin, C. Negrevergne, and R. Laflamme, Phys. Rev. Lett. **95**, 250502 (2005).
[43] J. S. Hodges, P. Cappellaro, T. F. Havel, R. Martinez, and D. G. Cory, Phys. Rev. A **75**, 042320 (2007).
[44] D.-X. Wei *et al.*, Chin. Phys. **13**, 817 (2004).
[45] Z. L. Madi, R. Brüschweiler, and R. R. Ernst, J. Chem. Phys. **109**, 10603 (1998).
[46] X. Wang, Z. Sun, and Z. D. Wang, e-print arXiv:0803.2940v2.
[47] M.-F. Yang, Phys. Rev. B **76**, 180403(R) (2007).
[48] H. T. Quan and F. M. Cucchietti, e-print arXiv:0806.4633v1.